Metastable and field-induced ferroelectric response in antiferroelectric lead zirconate thin film studied by the hyperbolic law and third harmonic response

Kevin Nadaud, Caroline Borderon, Raphaël Renoud, Micka Bah, Stephane Ginestar, Hartmut W Gundel

Metastable and Field-Induced Ferroelectric Response in Antiferroelectric Lead Zirconate Thin Film Studied by the Hyperbolic Law and Third Harmonic Response

Kevin Nadaud,[1, a)] Caroline Borderon,[2, b)] Raphaël Renoud,[2] Micka Bah,[1] Stephane Ginestar,[2] and Hartmut W. Gundel[2]

[1)] *GREMAN UMR 7347, Université de Tours, CNRS, INSA-CVL, 16 rue Pierre et Marie Curie, 37071 Tours, France*

[2)] *Nantes Université, CNRS, IETR UMR 6164, 44000 Nantes, France*

In this paper, the field-induced residual ferroelectricity in antiferroelectric lead zirconate thin films has been studied by impedance measurements together with a hyperbolic law analysis, which permits us to extract the different contributions to the material's complex permittivity. By measuring the Rayleigh coefficient α_r it appears that the residual ferroelectricity is considerably enhanced when the sample has been previously exposed to an electric field close to the antiferroelectric to ferroelectric transition field. This indicates that a part of the material remains ferroelectric after the antiferroelectric-ferroelectric backwards transition, which constitutes an additional contribution to polarization. Consequently a higher domain wall density and mobility can be observed. Measurements after exposition to thermal treatment show this ferroelectric response is metastable.

Keywords: Antiferroelectric, residual ferroelectricity, domain wall, impedance spectroscopy, metastable, hyperbolic analysis

[a)] Author to whom correspondence should be addressed: kevin.nadaud@univ-tours.fr

[b)] Electronic mail: caroline.borderon@univ-nantes.fr

I. INTRODUCTION

Antiferroelectric materials present a great interest for energy storage applications[1–3]. When a large electric field is applied to an ideal antiferroelectric, a transition to the ferroelectric phase occurs and the material comes back to the antiferroelectric state when the electric field is released, resulting in the double hysteresis in the polarization versus electric field loop[1,4,5]. The antiferroelectric-ferroelectric transition, however, may be irreversible for some compounds[6–10], and the material stays in the ferroelectric phase. In this case, the double hysteresis loop disappears in favor of a ferroelectric loop for successively applied cycles. Even in the case of a reversible antiferroelectric to ferroelectric transition, some weak ferroelectricity at zero electric field may contribute to the polarization in the material due to an unbalanced antiparallel shift of the oxygen atoms along the [001] direction[11].

For storage applications, a ferroelectric contribution to the polarization in an antiferroelectric material is undesirable since it increases switching losses and thus limits the efficiency of the component. In antiferroelectric materials based on lead zirconate ($PbZrO_3$, PZO) the residual ferroelectric contribution has been extensively studied[11–14] and is also called weak ferroelectricity. This residual ferroelectricity can be investigated using various methods as for example the observation of a current peak at low fields when measuring $I(E)$ loops at high fields (i.e. above the antiferroelectric to ferroelectric transition)[12,13] or the presence of a ferroelectric hysteresis loop $P(E)$ at low fields (i.e. below the antiferroelectric to ferroelectric transition)[11]. Impedance spectroscopy can be employed in order to see an eventual increase of the relative permittivity when the measuring electric field increases, i.e. observing a non-linear dielectric response, which indicates a ferroelectric domain wall pinning/unpinning contribution[1,4,14,15].

For a ferroelectric material containing domain walls, at sub-switching electric fields, the polarization can be described using the following expression:[16]

$$P = \varepsilon_0 \left(\varepsilon_{r-l} + \alpha_r E_0\right) E \pm \frac{\varepsilon_0 \alpha_r}{2} \left(E_0^2 - E^2\right) + \dots \tag{1}$$

with ε_{r-l} and α_r the lattice and the irreversible domain wall contributions (also called pinning/unpinning), respectively. The sign + stands for the decreasing and the sign − for the increasing part of the alternating field. The second term reflects the hysteretic contribution of the domain wall to the polarization. This non-linear expression of the polarization gives the following Fourier series decomposition when the applied electric field is

$E(t) = E_0 \sin(\omega t)$:

$$P(t, E_0) = \varepsilon_0 (\varepsilon_{r-l} + \alpha_r E_0) E_0 \sin(\omega t) - \frac{4\varepsilon_0 \alpha_r E_0^2}{3\pi} \cos(\omega t) - \frac{4\varepsilon_0 \alpha_r E_0^2}{\pi} \left[\frac{1}{15} \cos(3\omega t) - \frac{1}{105} \cos(5\omega t) + \dots \right] \quad (2)$$

The irreversible domain wall motion contribution is thus out-of-phase with the measuring electric field in the case of an ideal material. In order to describe a real material, equation (1) can contain additional terms, reflecting the degree of randomness of the energy profile,[17] and in that case, the harmonics may not be purely out-of-phase. For this reason, the non-linear response of a ferroelectric material can be investigated by extracting the phase of the third-harmonic contribution to the polarization and its evolution with the measuring field amplitude, which gives information on the hysteretic or an-hysteretic character of the domain wall motion[17–19].

On the other hand, recent work on PZO and PZO-based materials claim the possibility of a ferrielectric (FiE) phase structure[20–22] which may explain the non-null polarization zero field. Those studies predict the FiE phase, with an up-up-down orientation, is more stable than the FE phase at room temperature and also slightly more stable than the up-up-down-down pattern commonly admitted for PZO. It has been pointed out that the presence of a non-zero remnant polarization depends on the film orientation[22,23]. Yao *et al.* suggest that this comes from a ferrielectric phase which is anisotropic (similar to a ferroelectric phase) along specific crystallographic directions and behaves like an antiferroelectric along others[22]. The existence of the FiE phase has been experimentally confirmed by transmission electron microscopy in PZO/$SrTiO_3$ thin films deposited by pulsed laser deposition (PLD)[24]. The authors show that FE clusters can be contained in the AFE phase. Moreover, depending on the electric field, the FiE phase seems to be more stable than the AFE and FE state. Another study on epitaxial PZO grown by PLD shows that the up-up-down-down orientation is obtained but with an imperfect polarization compensation in adjacent cells[25]. The presence of a weak ferroelectricity is confirmed by the presence of a current peak at low fields while measuring $I(E)$ loops and second-harmonic generation characterizations. All those studies highlight the difficulty to precisely know the ground state of PZO, and, even with the conventional up-up-down-down arrangement, ferroelectric clusters[24] or a non-uniform local polarization orientation[25] may be present.

In the present study, the reversible antiferroelectric to ferroelectric transition is investi-

gated in PZO thin films to see the part of the material that exhibits a ferroelectric response. Using impedance measurements coupled with a hyperbolic law analysis, the different contributions to the permittivity have been decomposed and show an increase of the domain density and reduced the domain wall pinning/unpinning when a large electric field is applied and hence an enhancement of the residual ferroelectricity. The phase of the third-harmonic contribution to the polarization has been measured after applying various electric field amplitudes, too. Even if we cannot exclude the possibility that the material studied in the current paper can be in a ferrielectric phase, we will use a more generic way to name the phenomena (non-zero polarization and dielectric non-linearity), like ferroelectric behavior/response or weak ferroelectricity, which later has been widely used in the literature.

II. EXPERIMENTS

The lead zirconate $PbZrO_3$ (PZO) thin films are prepared by a sol-gel process[1,4,26]. The solution of 0.5 M concentration is deposited at 4000 rpm during 25 s by a multi-step spin coating process on an alumina substrate previously coated with a titanium and a platinum layers to form the bottom electrode. Each layer is annealed in a preheated open-air furnace at 650 °C during 10 min in order to obtain the perovskite structure. Twelve layers result in an overall film thickness of 800 nm. Square platinum electrodes of 0.1 mm width are deposited by RF magnetron sputtering in order to realize a Metal-Insulator-Metal (MIM) capacitor for the dielectric characterizations of the fabricated thin films.

X-ray diffraction (XRD) was performed for phase identification using a Siemens D5000 diffractometer with CuKα radiation. The X-ray diffraction pattern of PZO thin film is shown in Fig. 1. The peaks corresponding to the PZO perovskite structure are well visible and are indexed according to the pseudo-cubic crystallographic structure. The lead zirconate thin films are oriented along the (100) crystallographic plane at around 99% by taking into account the crystallographic orientation factor $\alpha_{hkl} = I_{hkl}/I_{total}$[27,28], where I_{hkl} corresponds to the peak intensity of the selected plane and I_{total} is the sum of all diffraction peaks. Obtaining this orientation on polycrystalline alumina substrate is due to a most thermodynamically favorable growth direction[29,30]. No parasite peak and no evidence of any secondary phase formation is visible.

The dielectric characterization method is similar to what has been used in Ref. 31 and

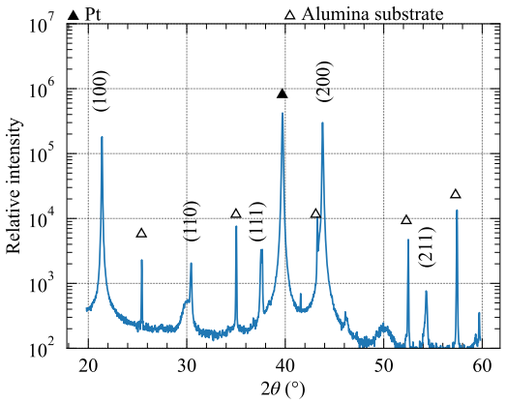

Figure 1. X ray diffraction pattern of the $PbZrO_3$ thin film.

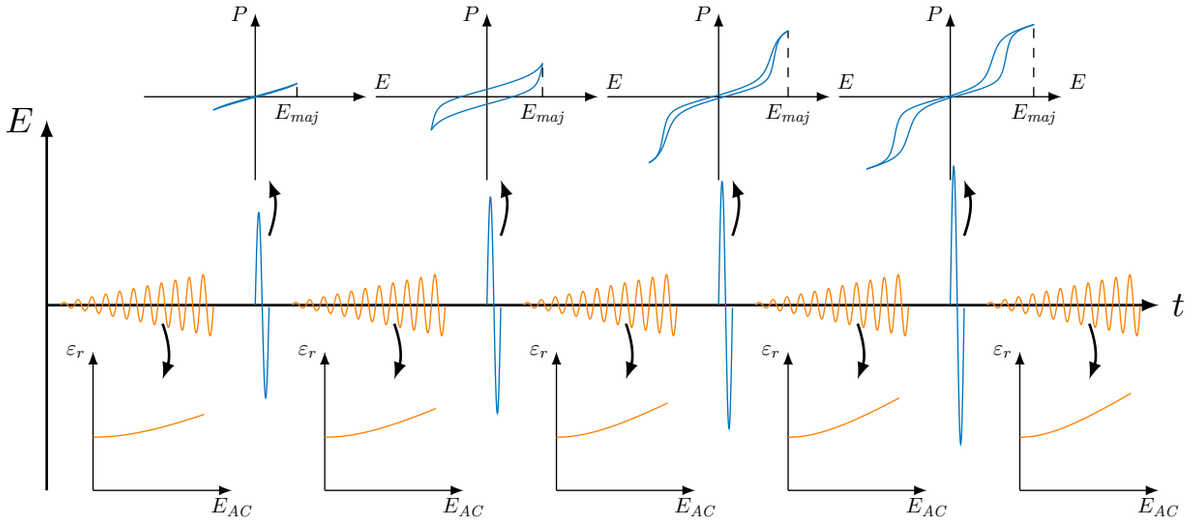

Figure 2. Description of the experimental protocol used for measuring the threshold electric field which enhances the ferroelectric contribution to the dielectric permittivity. $P(E)$ loops are obtained while increasing the electric field amplitude (blue curves). Between each major $P(E)$ loop (E_{maj}), impedance measurement as a function of the measuring field E_{AC} and hyperbolic analysis is done (orange curves).

was conducted at room temperature, i.e. $T = 25\,°C$ All the impedance measurements were done at an excitation signal frequency of 1 kHz, since previous work on PZO shows only a small decay of the dielectric permittivity when the frequency increases but no dielectric relaxation is visible between 100 Hz and 1 MHz[1] which is valid for all its contributions[26]. The current is measured as a function of time while applying an alternating voltage at 1 kHz and

the polarization is computed with the TF2000 analyzer software by numerical integration. In addition to the first harmonic study, giving access to the relative permittivity for which the computation is detailed further down, the non-linear response has been investigated by analyzing the third-harmonic phase angle.

For the hyperbolic and third-harmonic phase angle analysis, the measured current waveform has been fitted by $i(t) = \sum_{k=1}^{3} I_k \sin(k\omega t + \theta_{I_k})$ and the applied voltage by $v(t) = V \sin(\omega t + \theta_V)$ The first harmonic current and the applied voltage are used for the computation of the complex impedance:[4,31]

$$Z = \frac{|V|}{|I_1|} \exp\left(j\left(\theta_V - \theta_{I_1}\right)\right) \tag{3}$$

with j the imaginary unit. The complex capacitance C^* hence can be derived from the complex impedance:

$$C^* = \frac{1}{j\omega Z} = \frac{|I_1|}{\omega |V|} \exp\left(j\left(\theta_{I_1} - \theta_V - \frac{\pi}{2}\right)\right) \tag{4}$$

ω the angular frequency of the measuring voltage. The k-th harmonic phase angle extraction is similar and its value can be obtained using the following expression:

$$\delta_k = \theta_{I_k} - k\theta_V - \frac{\pi}{2} \tag{5}$$

In our case, we focus on the third-harmonic since its extraction is easier than for higher order harmonics due to a larger amplitude (2).

Even if the system in not symmetric in terms of the electrode configuration, the electric field distribution can be considered homogeneous between the electrodes due to the difference in terms of form factor (800 nm film thickness vs 100 µm electrode width). Those conditions allow to use the parallel plate formula for calculating the material relative permittivity ε_r^*:

$$\varepsilon_r^* = \frac{t}{S\varepsilon_0} C^*, \tag{6}$$

with t the thickness of the film, S the surface of the electrodes and ε_0 the vacuum permittivity. In the present case, the electrodes are sufficiently thick in order to limit the effect of the series resistance on the measured impedance. No relaxation is visible in the considered frequency range which permits us to directly use the impedance to compute the capacitance, otherwise, a more complex model needs to be used[32,33].

In the studied measurement configuration, the active area under the top electrode is surrounded by non-active material which affects the electrical and non-linear response (lower

value of the irreversible domain wall contribution) by a clamping effect[34–36]. The effect of the clamping shall be investigated in another study.

III. RESULTS AND DISCUSSION

In part III A, the general (ferroelectric) behavior of the antiferroelectric thin films is studied. Then, in part III B, impedance measurements is done after each $P(E)$ loop while increasing the applied field in order to study the enhancement effect at low fields. The evolution of the permittivity and hence the ferroelectric phase is examined, considering more particularly domain wall motion effects. Part III C focuses on the hyperbolic law analysis which used in order to decompose the material's complex permittivity into its lattice and domain wall (vibration and pinning/unpinning) contribution, and thus to precisely determine if the enhancement of the ferroelectric phase is due to a particular applied electric field. In the last part III D, exposition of the thin films to a higher temperature allows to verify if the observed weak ferroelectricity subsists or vanish after the thermal treatment, thus determining if the field-induced ferroelectricity is metastable.

A. $P(E)$ loops

In order to determine the evolution of the ferroelectric behavior, $P(E)$ major loops with increasing electric field amplitude have been measured on a virgin sample. The amplitude of the major electric field has been varied from $150\,\mathrm{kV\,cm^{-1}}$ to $875\,\mathrm{kV\,cm^{-1}}$ with an increment of $25\,\mathrm{kV\,cm^{-1}}$. The resulting $P(E)$ major loops are shown in Fig. 3.

The first series of measurements of the polarization versus electric field loops on a pristine sample are shown in Fig. 3a. The typical double hysteresis of an antiferroelectric material is well visible. The maximum value of polarization is $26\,\mu\mathrm{C\,cm^{-2}}$ which is close to the value reported for PZO thin films[37]. The antiferroelectric to ferroelectric and ferroelectric to antiferroelectric transition fields are respectively $E_{AF}^{+} = 628\,\mathrm{kV\,cm^{-1}}$ and $E_{FA}^{+} = 244\,\mathrm{kV\,cm^{-1}}$ for positive and $E_{AF}^{-} = -580\,\mathrm{kV\,cm^{-1}}$ and $E_{FA}^{-} = -229\,\mathrm{kV\,cm^{-1}}$ for negative electric fields. A rapid increase of the polarization is visible when the driving field magnitude reaches the antiferroelectric to ferroelectric transition, curves between $550\,\mathrm{kV\,cm^{-1}}$ and $650\,\mathrm{kV\,cm^{-1}}$. When repeating the measurement for a second time, similar values for the maximum polar-

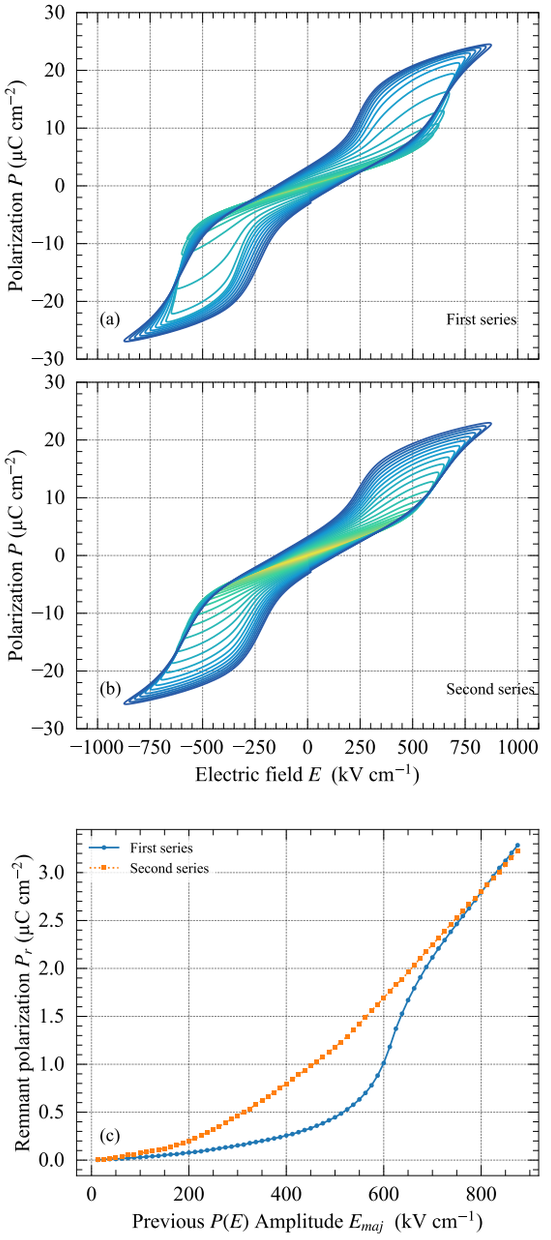

Figure 3. $P(E)$ loops for different value of the maximum electric field for the first (a) and the second (b) series of measurement. Remnant polarization for the two series (c).

ization and transition fields are obtained (Fig. 3b). The sharp increase of the polarization above the antiferroelectric to ferroelectric transition field is not visible and the curves are more regularly spaced.

The remnant polarization has been extracted for each measurement and is reported in Fig. 3c. For the first series, the remnant polarization shows a sharp increase around

$600\,\mathrm{kV\,cm^{-1}}$, a similar field as observed for the strong increase of the polarization. For the second series, the remnant polarization at fields below the antiferroelectric to ferroelectric transition, is higher than for the first series and enhancement regularly, without the sharp increase around $600\,\mathrm{kV\,cm^{-1}}$. In order to verify whether the change of remnant polarization is linked to an increase of the ferroelectric response, impedance measurements as function of the AC measuring field have been carried out and are shown in the next part.

B. Permittivity evolution

Between each $P(E)$ major loop measurement, the permittivity of the film has been determined as a function of the amplitude of the measuring field E_{AC} to see the evolution of the ferroelectric contribution (Fig. 2). The amplitude of this measuring field, swept from $1.25\,\mathrm{kV\,cm^{-1}}$ to $125\,\mathrm{kV\,cm^{-1}}$, has been kept sufficiently small to stay at sub-switching level, i.e. below the antiferroelectric-ferroelectric transition field[16,38].

The real and the imaginary parts of the permittivity as a function of the amplitude E_{AC} used for the impedance analysis are shown in Fig. 4, for an increasing amplitude of the previously applied major field E_{maj}. For a better readability, only few E_{maj} value are shown, all measured data are given in the supplementary material. For a virgin sample, i.e. before applying any major electric field (noted $E_{maj} = 0\,\mathrm{kV\,cm^{-1}}$) and up to $E_{maj} \simeq 500\,\mathrm{kV\,cm^{-1}}$, the real and imaginary parts of the relative permittivity evolve only little as a function of the major electric field. The observed rather linear increase with the measuring field is due to the ferroelectric domain wall motion contribution[16,38].

Between $E_{maj} = 500\,\mathrm{kV\,cm^{-1}}$ and $E_{maj} = 700\,\mathrm{kV\,cm^{-1}}$, the permittivity at small AC measuring fields shows a small increase, from 122 to 128 for the real part and 4.4 to 5.4 for the imaginary part. At higher AC fields, the slope of the permittivity with the measuring field which is higher can be attributed to an increase of the domain wall pinning/unpinning, signature of a ferroelectric behavior. Above $E_{maj} = 700\,\mathrm{kV\,cm^{-1}}$, the slope increase is negligible indicating that the ferroelectricity has been established and is not enhanced anymore by a higher applied electric field of the $P(E)$ major loop.

The dielectric non-linearity, signature of ferroelectric domain wall motions, have been already observed in antiferroelectric materials such as PZO[4,15,22,26] and in $(\mathrm{Pb,La})(\mathrm{Zr,Ti})\mathrm{O_3}$[14]. One can note that the measuring electric field is small compared to the transition field (from

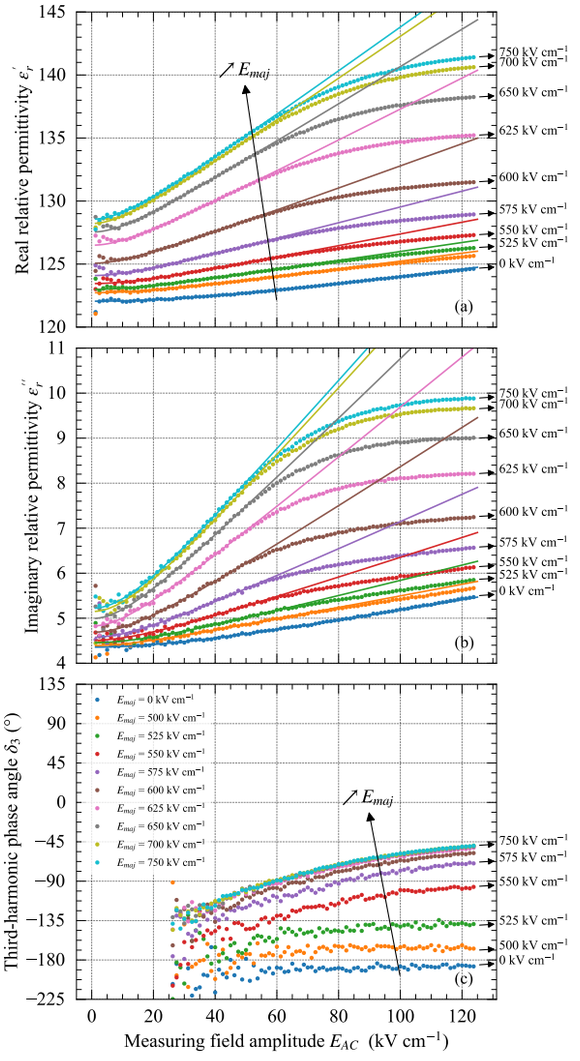

Figure 4. Real (a) and imaginary (b) parts of the relative permittivity and phase of the third-harmonic contribution to the polarization (c), as a function of the measuring field amplitude obtained after each $P(E)$ cycle with successively increasing electric field amplitudes E_{maj}. The dots are the experimental results and the solid lines correspond to the hyperbolic fits (7).

AFE to FE phase) and the current associated to those transition does not contribute to the permittivity. In addition, only ferroelectric domain walls contribute to this increase of relative permittivity, since antiferroelectric domain wall motion cannot move under the action of an homogeneous electric field[39].

The third-harmonic phase angle is reported in Fig. 4c as a function of the AC measuring electric field for different values of the previously applied major field E_{maj}. In the case of a

Table I. Numerical values of the coefficients extracted with the hyperbolic law from the curves presented in Fig. 4.

	Real part			Imaginary part		
E_{maj}	Lattice ε'_{r-l}	Vibration ε'_{r-rev}	Pinning/Unpinning α'_r ($\mathrm{cm\,kV^{-1}}$)	Lattice ε''_{r-l}	Vibration ε''_{r-rev}	Pinning/Unpinning α''_r ($\mathrm{cm\,kV^{-1}}$)
$0\,\mathrm{kV\,cm^{-1}}$	120.3 ± 0.1	1.8 ± 0.1	0.0327 ± 0.0008	3.89 ± 0.06	0.47 ± 0.07	0.0121 ± 0.0004
$500\,\mathrm{kV\,cm^{-1}}$	121.9 ± 0.1	0.8 ± 0.1	0.032 ± 0.001	4.18 ± 0.06	0.21 ± 0.08	0.0130 ± 0.0007
$550\,\mathrm{kV\,cm^{-1}}$	122.6 ± 0.1	0.9 ± 0.2	0.047 ± 0.002	4.1 ± 0.1	0.4 ± 0.1	0.022 ± 0.001
$575\,\mathrm{kV\,cm^{-1}}$	123.1 ± 0.1	1.0 ± 0.2	0.063 ± 0.002	4.0 ± 0.1	0.5 ± 0.2	0.031 ± 0.002
$600\,\mathrm{kV\,cm^{-1}}$	123.83 ± 0.09	1.2 ± 0.1	0.089 ± 0.001	3.9 ± 0.1	0.8 ± 0.1	0.044 ± 0.001
$625\,\mathrm{kV\,cm^{-1}}$	124.8 ± 0.1	1.7 ± 0.2	0.124 ± 0.002	4.0 ± 0.1	0.8 ± 0.1	0.056 ± 0.001
$650\,\mathrm{kV\,cm^{-1}}$	125.6 ± 0.1	1.9 ± 0.2	0.149 ± 0.002	3.99 ± 0.09	1.0 ± 0.1	0.067 ± 0.001
$700\,\mathrm{kV\,cm^{-1}}$	126.2 ± 0.1	2.1 ± 0.1	0.168 ± 0.001	3.9 ± 0.1	1.2 ± 0.1	0.076 ± 0.001
$750\,\mathrm{kV\,cm^{-1}}$	126.1 ± 0.1	2.5 ± 0.2	0.176 ± 0.002	3.9 ± 0.1	1.3 ± 0.1	0.078 ± 0.002

virgin sample, the phase is close to $-180°$, which corresponds to a non-hysteretic contribution of the domain wall motion to the polarization, similar to what is observed for hard Fe-doped PZT[18]. In this case, it is mainly domain wall vibration (reversible domain wall motion) as deep pinning centers limit the domain wall . Between $E_{maj} = 500\,\mathrm{kV\,cm^{-1}}$ and $E_{maj} = 600\,\mathrm{kV\,cm^{-1}}$, the phase of the third-harmonic progressively goes to another regime. This regime corresponds to a phase angle which increases from $-135°$ to $-45°$ when the measuring field E_{AC} increases from $25\,\mathrm{kV\,cm^{-1}}$ to $125\,\mathrm{kV\,cm^{-1}}$, similar to what is observed for soft Nb-doped PZT[18]. This indicates a progressive change from a non-hysteretic contribution of the domain wall motion to the polarization at low measuring fields (reversible, domain wall vibration) to a hysteretic contribution to the polarization (irreversible, domain wall pinning/unpinning) at high measuring fields. The change of the domain wall motion regime also indicates a change of the pinning center depth. In the present case, the non-linearity at E_{AC} field below $25\,\mathrm{kV\,cm^{-1}}$ is too weak to allow a proper estimation of the third-harmonic phase angle. Consequently, the expected limit of $-180°$ at low E_{AC} fields can be seen only in the case of applied major fields $E_{maj} \leq 525\,\mathrm{kV\,cm^{-1}}$, but the nominal value seems to be

approached also at higher fields. Instead of the expected phase angle of $-90°$, characteristic an irreversible domain wall motion contribution, the observed limit at high E_{AC} field is closed to $-45\,\mathrm{kV\,cm^{-1}}$ which is attributed to a saturation-like component[17,18]. The saturation is well visible from the evolution of the real part of the dielectric permittivity that shows a deviation from the linear Raleigh increase at large E_{AC} fields.

Due to this transition from reversible to irreversible contributions when E_{AC} changes, the hyperbolic law[38,40] is chosen for the domain wall motion contribution to the permittivity analysis. This model is an extension of the Rayleigh law and considers in the same expression, both the reversible and irreversible contributions to the dielectric permittivity.

C. Hyperbolic analysis

In order to determine the different contributions to the permittivity (lattice, domain wall vibration, pinning/unpinning) the hyperbolic law[38,40] is used:

$$\varepsilon_r = \varepsilon_{r-l} + \sqrt{\varepsilon_{r-rev}^2 + (E_{AC}\alpha_r)^2}, \tag{7}$$

where ε_{r-l} is the lattice contribution to the permittivity, ε_{r-rev} and α_r correspond respectively to domain wall vibrations and domain wall pinning/unpinning (jump). The coefficients are extracted using Levenberg-Marquat method, which consists of minimizing the quadratic error. In order to determine the parameters, data deviating from the linear region at high fields are not taken into account (i.e. $E_{AC} \geq 85\,\mathrm{kV\,cm^{-1}}$ for $E_{maj} = 0\,\mathrm{kV\,cm^{-1}}$ and $E_{AC} \geq 50\,\mathrm{kV\,cm^{-1}}$ for $E_{maj} = 875\,\mathrm{kV\,cm^{-1}}$).

The ferroelectric residual phase has already been shown in the literature using Rayleigh analysis (which consider a linear increase)[14]. The hyperbolic analysis allows in addition to obtain respectively information on the domain wall vibration contribution, an indicator of the domain wall density[4,41,42] and the threshold field which points out the degree of wall pinning in the material[43]. The different contributions obtained are shown Fig. 5

At low fields, the lattice contribution to polarization is constant (Fig. 5a), starts to increase around $E_{maj} = 200\,\mathrm{kV\,cm^{-1}}$, and reaches its maximum value around $E_{maj} = 650\,\mathrm{kV\,cm^{-1}}$. The variation of the real part ε_r' is rather small (4 %) and the imaginary part ε_r'' stays constant.

The real and imaginary parts of the domain wall pinning/unpinning contribution are shown in Fig. 5b. Contrary to the lattice parameter, a large increase of the α_r' and α_r''

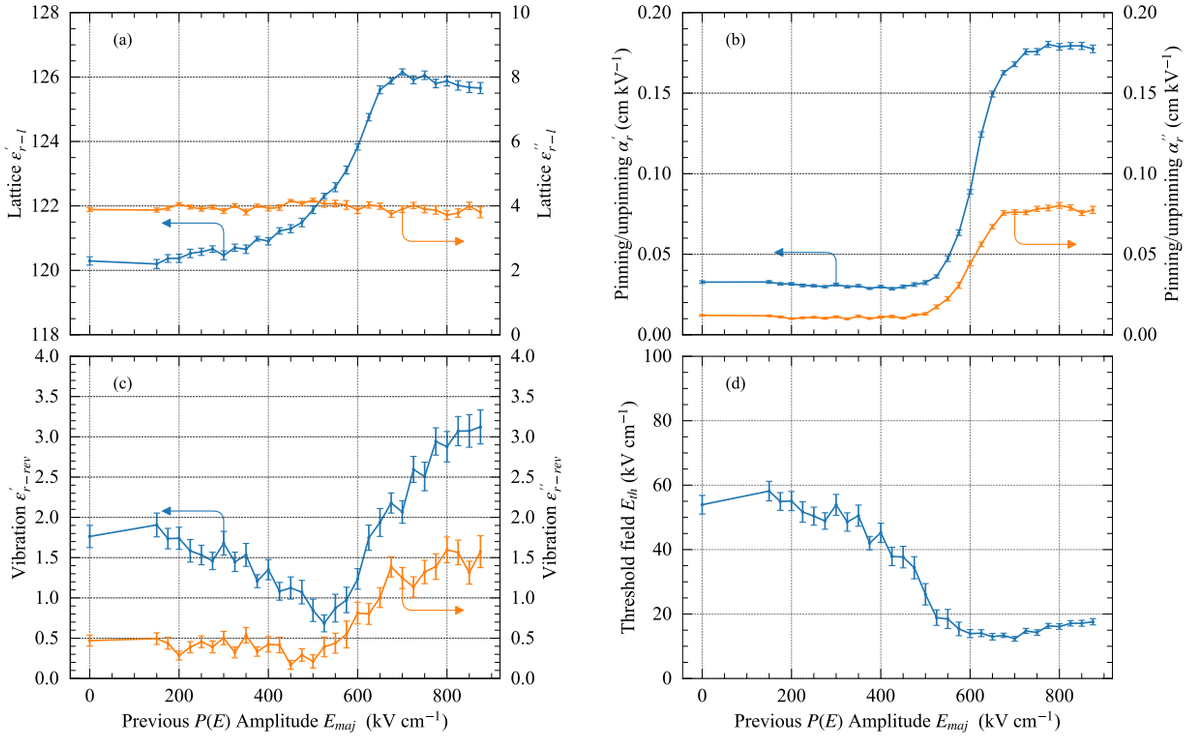

Figure 5. Real and imaginary parts of the different contributions to the dielectric permittivity, as a function of the previously applied $P(E)$ loop amplitude E_{maj}: lattice (a), domain wall pinning/unpinning (b) and domain wall vibration (c). The retrieved threshold field E_{th} as a function of E_{maj} (d).

values can be seen between 550 kV cm^{-1} and 700 kV cm^{-1}, which are multiplied by a factor of 5.4 and 6.4 respectively. This confirms that the ferroelectric behavior is enhanced when applying a major electric field E_{maj} above 500 kV cm^{-1} and corresponds to what has been previously seen in Fig. 4 since α_r represents the slope of the permittivity rise as a function of the measuring field. For the studied PZO sample, α'_r is small, 3 orders of magnitude smaller than for ferroelectric $Pb(Zr_{0.52}Ti_{0.48})O_3$[44,45] and of the same order of magnitude than in $Ba_{0.80}Sr_{0.20}TiO_3$[40,41]. Nevertheless, the Rayleigh parameter α'_r is one order of magnitude higher than for heavily constrained $Pb(Zr_{0.20}Ti_{0.80})O_3$ thin film[46] for which almost no domain wall pinning/unpinning is visible due to a low domain density and high threshold field. In the present case, the ferroelectric contribution is largely enhanced by the application of a high electric field which is not the case for $(Pb, La)(Zr, Ti)O_3$[14] where the application of a

large electric field only slightly increases the Rayleigh coefficient (2 %).

Analysis with the hyperbolic law also allows extracting the domain wall vibration contribution, the real and imaginary parts, which are shown in Fig. 5c. The domain wall vibration parameter ε'_{r-rev} is small confirming a low ferroelectric domain wall density.

For small electric fields E_{maj}, the domain wall vibration parameter decreases, corresponding to the diminution of the domain wall density due to the onset of the orientation of the ferroelectric domains in the direction of the electric field and thus to domain merging by removing of the domain walls[4,47]. After a local minimum at a major electric field around $500\,\mathrm{kV\,cm^{-1}}$, the domain wall vibration contribution increases (up to a level higher than the initial value), confirming an enlargement of the ferroelectric clusters in the antiferroelectric matrix after application of high field E_{maj} loops. One can note that the field range which triggers the ferroelectric behavior is close to the antiferroelectric to ferroelectric transition ($E^{+}_{AF} = 628\,\mathrm{kV\,cm^{-1}}$ and $E^{-}_{AF} = -580\,\mathrm{kV\,cm^{-1}}$) indicating that the residual ferroelectric has transition field closely related to the antiferroelectric behavior of the material, as already noticed using First Order Reversal Curve (FORC) measurements[4]. It seems that the residual ferroelectricity comes from some part of the material that switches to the ferroelectric state when a sufficiently high field is applied but does not go back to the antiferroelectric state when the field is released and hence remains in the ferroelectric state.

Using the domain wall vibration and pinning/unpinning parameters, a threshold field can be found:[38,46]

$$E_{th} = \frac{\varepsilon'_{r-rev}}{\alpha'_r} \tag{8}$$

which is shown as a function of the previously major electric field E_{maj} in Fig. 5d and represents the degree of wall pinning in the material[43].

For small major electric fields E_{maj}, the threshold field is almost constant around $55\,\mathrm{kV\,cm^{-1}}$, indicating a strong pinning of the domain walls, similarly to what has been found for heavily constrained PZT[46]. With increasing major electric field, the threshold field decreases indicating a larger mobility of the domain walls. In this region, the enhancement of the dielectric non-linearity (increase of the pinning/unpinning parameter α'_r) is correlated to the facility to unpin domain walls but not to a higher domain wall density since the domain wall vibration parameter ε_{r-rev} remains small. Above $600\,\mathrm{kV\,cm^{-1}}$, the threshold field is rather stable, about three times smaller than for a virgin sample. Nevertheless, it is still one order of magnitude higher than in the ferroelectric compounds PZT[43] or BST[48]

indicating deep pinning centers and a low mobility of the domain wall.

The low domain wall density and their higher mobility confirm the deviation to the linear regime, visible at lower measuring field amplitude E_{AC} (Fig. 4), is due to vibration of the wall into small ferroelectric clusters[4,26]. A higher mobility, lower threshold field, corresponds to a lower defect depth and the domain wall vibrates for a lower field once the ferroelectricity is enhanced.

The number of cycle of the different contributions to the dielectric permittivity has been investigated up to 100 cycles and no wake up effect of fatigue has been seen (see Supplementary material).

D. Persistence of the ferroelectricity

In the previous part, we show that a residual ferroelectric phase appears in some region of the thin film, not switching back to the antiferroelectric state after the release of the electric field while doing $P(E)$ loops. In order to verify if this residual ferroelectricity is persistent or metastable, thermal treatment and impedance measurement as a function of the measuring field amplitude, coupled with hyperbolic analysis, have been done. The 4 steps measurement protocol has been carried out:

1. Impedance measurement at the ambient temperature on a fresh sample (indicating (F) in Fig. 6)

2. Application of a high electric field major loop $P(E)$ in order to establish the residual ferroelectric phase and consecutive impedance measurements (indicated (M) in Fig. 6)

3. Exposition of the thin film to a heat treatment during 20 min at 150 °C and consecutive impedance measurements (indicated (T) in Fig. 6) at ambient temperature

4. Application again of the high electric field major loop $P(E)$ and consecutive impedance measurement (indicated (TM) in Fig. 6)

Likewise in the first part of our study, the application of a high electric field consists to a $P(E)$ loop with a major electric field amplitude of 875 kV cm^{-1}.

The real and imaginary parts of the permittivity as a function of the measuring electric field amplitude, for the described conditions, are presented in Fig. 6. Both parts have been

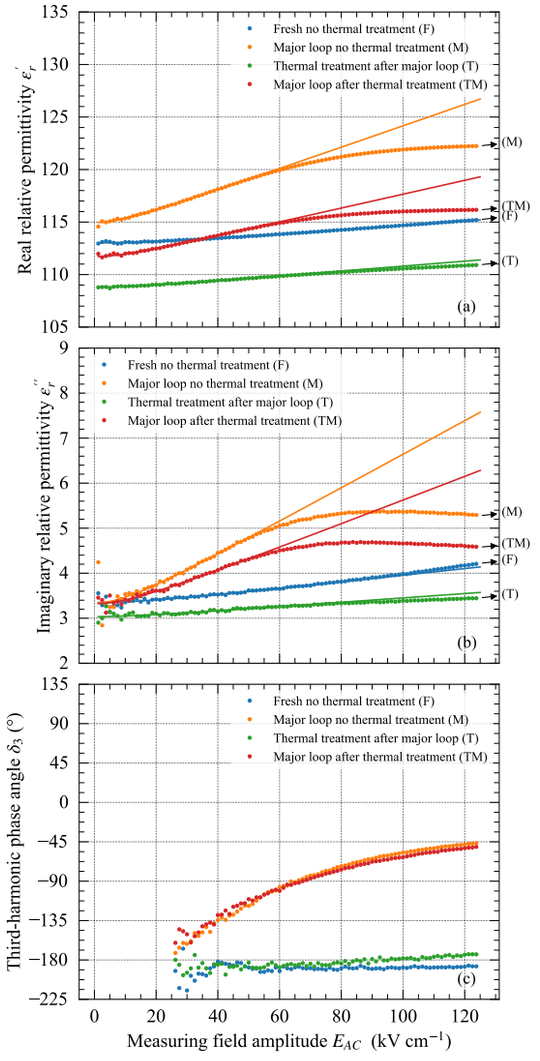

Figure 6. Real (a) and imaginary (b) parts of the relative permittivity and third harmonics phase angle (c), as a function of the measuring field amplitude, for conditions of cycling and thermal treatment.

fitted using the hyperbolic law (7) and the obtained parameter values are summarized in Table II. In the case of the fresh sample (step 1, curve (F) in Fig. 6), the real and imaginary parts of the permittivity show a small rise with the increasing measuring field due to a very weak ferroelectric contribution, as already seen previously. After exposition to a large electric field (step 2, curve (M) in Fig. 6), the increase of the permittivity is larger due to the field-induced ferroelectricity, visible by the higher values of ε'_{r-rev} and α'_r. Those both conditions are consistent with the measurement described in the parts III C.

Table II. Numerical values of the extracted coefficients using the hyperbolic laws of curves presented Fig. 6.

		Conditions			
	Contribution	Fresh no thermal treatment Curve (F)	Major loop no thermal treatment Curve (M)	Thermal treatment after major loop Curve (T)	Major loop after thermal treatment Curve (TM)
Real part	ε'_{r-l}	112.34 ± 0.06	113.85 ± 0.06	108.4 ± 0.1	110.95 ± 0.06
	ε'_{r-rev}	0.68 ± 0.07	1.11 ± 0.09	0.4 ± 0.1	0.77 ± 0.09
	α'_r ($\mathrm{cm\,kV^{-1}}$)	0.022 ± 0.001	0.103 ± 0.001	0.024 ± 0.001	0.067 ± 0.001
Imaginary part	ε''_{r-l}	3.19 ± 0.04	2.84 ± 0.08	2.95 ± 0.06	2.94 ± 0.08
	ε''_{r-rev}	0.16 ± 0.05	0.5 ± 0.1	0.09 ± 0.08	0.4 ± 0.1
	α''_r ($\mathrm{cm\,kV^{-1}}$)	0.008 ± 0.001	0.038 ± 0.001	0.005 ± 0.001	0.027 ± 0.001
Dissipation factors	$m_{\varepsilon_{r-l}}$	0.028 ± 0.001	0.025 ± 0.001	0.027 ± 0.001	0.027 ± 0.001
	$m_{\varepsilon_{r-rev}}$	0.23 ± 0.08	0.4 ± 0.1	0.2 ± 0.3	0.5 ± 0.1
	m_{α_r}	0.34 ± 0.02	0.37 ± 0.01	0.20 ± 0.03	0.40 ± 0.02
Threshold field	E_{th} ($\mathrm{kV\,cm^{-1}}$)	31 ± 2	11 ± 1	19 ± 4	12 ± 1

After exposition of the film to a thermal treatment (step 3, curve (T) in Fig. 6), the increase of the permittivity with the AC measuring field becomes very small, similar to the case of the fresh sample, indicating that the domain wall pinning/unpinning contribution to the permittivity is weak. The slope of the real part, corresponding to the pinning/unpinning parameter α'_r, is equal for the F and T curves which means that the residual ferroelectric contribution (induced in step 2) has been removed with the exposition of the sample to a thermal treatment. The ferroelectric domain wall density (indicated by the parameter ε'_{r-rev}) is smaller compared to the fresh sample since the ε'_{r-rev} value is equal to 0.4 and 0.68 respectively. This might be due to a migration of defects during the thermal treatment, which improve the antiferroelectric phase. After the thermal treatment, a lower value of the threshold field is observed ($19\,\mathrm{kV\,cm^{-1}}$ compared to $31\,\mathrm{kV\,cm^{-1}}$.), which is consistent with the lower domain wall density associated to a similar value of the domain wall pinning/unpinning coefficient α'_r. The ferroelectric domain walls hence seem to be in shallow

pinning centers and have a higher domain wall mobility. The dissipation factor m_{α_r} for the pinning/unpinning contribution is then lower than for the fresh sample due to the shallow pinning center and the lower interaction between domain walls, which is consistent with the lower domain wall density.

Finally, when exposing the thin film once more to a high electric field (step 4, curve (TM) in Fig. 6), the increase of the permittivity with the measuring field is again well visible, but the ferroelectric activity is smaller than for the first exposition of the fresh sample to a large electric field, represented by a lower Rayleigh coefficient ($\alpha'_r = 0.067\,\mathrm{cm\,kV^{-1}}$ vs $0.103\,\mathrm{cm\,kV^{-1}}$). This lower ferroelectric activity is due to the lower domain wall density since, after the thermal treatment and then the exposition to an electric field, the ε'_{r-rev} value is approximately two times lower than before (0.77 vs 1.11) whereas the threshold field is similar ($12\,\mathrm{kV\,cm^{-1}}$ vs $11\,\mathrm{kV\,cm^{-1}}$) indicating that the pinning centers are not deeper after applying a large electric field.

The third-harmonic phase angle δ_3 has been determined for each step of the measurement protocol and is shown in Fig. 6c. The evolution with the measuring field amplitude EAC is similar in the case of the fresh thin film and after the thermal treatment (curve (F) and (T), respectively). The phase angle is very close to $-180°$ for all measuring fields, indicating deep pinning of the domain walls and thus limiting the irreversible contribution (pinning/unpinning). After exposition of the thin film to the major $P(E)$ loop, reversible domain wall motion at low measuring fields still occurs but irreversible domain wall motion becomes more important at high fields as indicated by a phase angle δ_3 which increases up to 45°. The behavior of the third-harmonic phase angle is similar for step 2 and 4 which means that the field-induced ferroelectricity appears again after the application of a large electric field.

The measurement described in this part indicates that the field induced ferroelectricity is metastable. Ferroelectricity disappears after the exposition of the sample to a thermal treatment but can be partially restored by the application of a large electric field which has been also noticed for lanthanum-doped lead zirconate titanate stannate[8]. The major difference in our work is that the antiferroelectric behavior is mostly restored when the field is removed in our work since the double hysteresis loop is well visible even for a sample already exposed to a high electric contrary to the typical ferroelectric $P(E)$ loop obtained ref. 8. The return to the antiferroelectric phase is consistent with the theoretical predictions

of Aramberri *et al*[20] as we observe that the ferroelectric phase is slightly less stable than the antiferroelectric state. Nevertheless, it needs some energy since the free energy difference between the two phases is small[49], provided by the thermal treatment, to allow reestablishing the antiferroelectric phase.

IV. CONCLUSION

In this paper, the evolution of the ferroelectric response in antiferroelectric PZO thin films has been studied using hyperbolic law and third-harmonic phase angle analysis. At low major electric fields E_{maj}, a large threshold field, indicating deep pinning centers and a small vibrating parameter ε'_{r-rev} are observed in the studied thin film. After the application of a major electric field $E_{maj} > 500\,\mathrm{kV\,cm^{-1}}$ in order to measure the polarization versus electric field loop $P(E)$ an enhancement of the ferroelectricity can be deduced from two observations: (i) the more important domain density, visible from the higher value of the domain wall vibration parameter ε'_{r-rev} (which is almost doubled, see Fig. 5c), and (ii) the smaller threshold field E_{th}, which is divided by more than 3 after the application of the high field E_{maj} (see Fig. 5d), indicating a higher mobility of domain walls. The third-harmonic phase angle analysis reveals that the domain wall are deeply pinned before the field exposition and the pinning degree is lower once a large field has been applied, which is consistent with a higher ferroelectric activity.

The transition occurs when the maximum applied electric field is close to the antiferroelectric to ferroelectric transition field (E_{AF}). As expected, this indicates that the polarization tends to be oriented when the electric field exceeds E_{AF}. When the electric field goes back to 0, some clusters still exhibit a ferroelectric response that is more important compared to the virgin sample and the ferroelectric to antiferroelectric phase transition is not complete.

The observed residual ferroelectricity, however, is not stable as the field induced ferroelectric response disappears once the film has been exposed to thermal treatment. Finally, it can be enhanced again by applying a large electric field, indicating the metastable character of the field-induced ferroelectric response in the antiferroelectric PZO thin film. The different contributions to the complex permittivity and hence the domain wall dynamic can be particularly well studied by using impedance measurements with hyperbolic law analysis, also providing information on the pinning center depth of the thin film.

DATA AVAILABILITY

The data that support the findings of this study are available from the corresponding author upon reasonable request.

SUPPLEMENTARY MATERIAL

See supplementary material for the permittivity and third-harmonics phase angle evolution for all previous major electric field and the effect of the number of cycle on the different contributions to the permittivity.

ACKNOWLEDGMENTS

This work has been performed with the means of the technological platform SMART SENSORS of the French region Pays de la Loire and with the means of the CERTeM (microelectronics technological research and development center) of French region Centre Val de Loire.

CONFLICT OF INTEREST

The authors declare no competing financial interest.

REFERENCES

[1]M. D. Coulibaly, C. Borderon, R. Renoud, and H. W. Gundel, Thin Solid Films **716**, 138432 (2020).

[2]M. Sharifzadeh Mirshekarloo, K. Yao, and T. Sritharan, Applied Physics Letters **97**, 142902 (2010).

[3]C. Liu, S. X. Lin, M. H. Qin, X. B. Lu, X. S. Gao, M. Zeng, Q. L. Li, and J.-M. Liu, Applied Physics Letters **108**, 112903 (2016).

[4]K. Nadaud, C. Borderon, R. Renoud, M. Bah, S. Ginestar, and H. W. Gundel, Applied Physics Letters **118**, 042902 (2021).

[5]S.-E. Park, M.-J. Pan, K. Markowski, S. Yoshikawa, and L. E. Cross, Journal of Applied Physics **82**, 1798 (1997).

[6]M.-H. Zhang, L. Fulanović, S. Egert, H. Ding, P. B. Groszewicz, H.-J. Kleebe, L. Molina-Luna, and J. Koruza, Acta Materialia **200**, 127 (2020).

[7]Y. Li, W. Cao, Q. Li, Q. Yan, J. Gao, F. Zhuo, X. Xi, Y. Zhang, and X. Chu, Applied Physics Letters **104**, 052912 (2014).

[8]T. Yang and X. Yao, Ceramics International **34**, 715 (2008).

[9]F. Zhuo, Q. Li, Y. Li, J. Gao, Q. Yan, Y. Zhang, X. Xi, X. Chu, and W. Cao, Journal of Applied Physics **121**, 064104 (2017).

[10]J. Gao, Q. Li, Y. Li, F. Zhuo, Q. Yan, W. Cao, X. Xi, Y. Zhang, and X. Chu, Applied Physics Letters **107**, 072909 (2015).

[11]X. Dai, J.-F. Li, and D. Viehland, Phys. Rev. B **51**, 2651 (1995).

[12]K. Boldyreva, D. Bao, G. L. Rhun, L. Pintilie, M. Alexe, and D. Hesse, Journal of Applied Physics **102**, 044111 (2007).

[13]L. Pintilie, K. Boldyreva, M. Alexe, and D. Hesse, Journal of Applied Physics **103**, 024101 (2008).

[14]Z. Luo, X. Lou, F. Zhang, Y. Liu, D. Chang, C. Liu, Q. Liu, B. Dkhil, M. Zhang, X. Ren, and H. He, Applied Physics Letters **104**, 142904 (2014).

[15]S. Bharadwaja, A. Laha, S. Halder, and S. Krupanidhi, Materials Science and Engineering: B **94**, 218 (2002).

[16]D. V. Taylor and D. Damjanovic, Journal of Applied Physics **82**, 1973 (1997).

[17]S. Hashemizadeh and D. Damjanovic, Applied Physics Letters **110**, 192905 (2017).

[18]M. Otoničar, M. Dragomir, and T. Rojac, Journal of the American Ceramic Society **105** (2022), 10.1111/jace.18623.

[19]M. I. Morozov and D. Damjanovic, Journal of Applied Physics **104**, 034107 (2008).

[20]H. Aramberri, C. Cazorla, M. Stengel, and J. Íñiguez, npj Computational Materials **7**, 1 (2021).

[21]Z. Fu, X. Chen, Z. Li, T. Hu, L. Zhang, P. Lu, S. Zhang, G. Wang, X. Dong, and F. Xu, Nature Communications **11**, 3809 (2020).

[22]Y. Yao, A. Naden, M. Tian, S. Lisenkov, Z. Beller, A. Kumar, J. Kacher, I. Ponomareva, and N. Bassiri-Gharb, Advanced Materials , 2206541 (2022).

[23]C. Milesi-Brault, N. Godard, S. Girod, Y. Fleming, B. El Adib, N. Valle, S. Glinšek, E. Defay, and M. Guennou, Applied Physics Letters **118**, 042901 (2021).

[24]R.-J. Jiang, Y. Cao, W.-R. Geng, M.-X. Zhu, Y.-L. Tang, Y.-L. Zhu, Y. Wang, F. Gong, S.-Z. Liu, Y.-T. Chen, J. Liu, N. Liu, J.-H. Wang, X.-D. Lv, S.-J. Chen, and X.-L. Ma, Nano Letters **23**, 1522 (2023), publisher: American Chemical Society.

[25]Y. Si, T. Zhang, Z. Chen, Q. Zhang, S. Xu, T. Lin, H. Huang, C. Zhou, S. Chen, S. Liu, Y. Dong, C. Liu, Y. Tang, Y. Lu, K. Jin, E.-J. Guo, and X. Lin, ACS Applied Materials & Interfaces **14**, 51096 (2022), publisher: American Chemical Society.

[26]M. D. Coulibaly, C. Borderon, R. Renoud, and H. W. Gundel, Applied Physics Letters **117**, 142905 (2020).

[27]Y. Zhao, H. Gao, X. Hao, and Q. Zhang, Materials Research Bulletin **84**, 177 (2016).

[28]W. Zhu, W. Ren, H. Xin, P. Shi, and X. Wu, Journal of Advanced Dielectrics **03**, 1350011 (2013).

[29]G.-T. Park, J.-J. Choi, C.-S. Park, J.-W. Lee, and H.-E. Kim, Applied Physics Letters **85**, 2322 (2004).

[30]K. G. Brooks, I. M. Reaney, R. Klissurska, Y. Huang, L. Bursill, and N. Setter, Journal of Materials Research **9**, 2540 (1994).

[31]K. Nadaud, C. Borderon, R. Renoud, M. Bah, S. Ginestar, and H. W. Gundel, Journal of Alloys and Compounds **914**, 165340 (2022).

[32]M. T. Becker, C. J. Burkhardt, R. Kleiner, and D. Koelle, Journal of Applied Physics **132**, 044104 (2022).

[33]T. Schenk, M. Hoffmann, M. Pešić, M. H. Park, C. Richter, U. Schroeder, and T. Mikolajick, Physical Review Applied **10** (2018), 10.1103/physrevapplied.10.064004.

[34]R. Keech, S. Shetty, M. A. Kuroda, X. Hu Liu, G. J. Martyna, D. M. Newns, and S. Trolier-McKinstry, Journal of Applied Physics **115**, 234106 (2014).

[35]F. Griggio, S. Jesse, A. Kumar, O. Ovchinnikov, H. Kim, T. Jackson, D. Damjanovic, S. Kalinin, and S. Trolier-McKinstry, Physical Review Letters **108**, 157604 (2012).

[36]L. M. Denis, G. Esteves, J. Walker, J. L. Jones, and S. Trolier-McKinstry, Acta Materialia **151**, 243 (2018).

[37]P. Ayyub, S. Chattopadhyay, R. Pinto, and M. S. Multani, Phys. Rev. B **57**, R5559 (1998).

[38]C. Borderon, R. Renoud, M. Ragheb, and H. W. Gundel, Applied Physics Letters **98**, 112903 (2011).

[39]K. Vaideeswaran, K. Shapovalov, P. V. Yudin, A. K. Tagantsev, and N. Setter, Applied Physics Letters **107**, 192905 (2015).

[40]K. Nadaud, C. Borderon, R. Renoud, and H. W. Gundel, Journal of Applied Physics **119**, 114101 (2016).

[41]K. Nadaud, C. Borderon, R. Renoud, and H. W. Gundel, Journal of Applied Physics **117**, 084104 (2015).

[42]K. Nadaud, M. Sadl, M. Bah, F. Levassort, and H. Ursic, Applied Physics Letters **120**, 112902 (2022).

[43]N. B. Gharb and S. Trolier-McKinstry, Journal of Applied Physics **97**, 064106 (2005).

[44]W. Zhu, I. Fujii, W. Ren, and S. Trolier-McKinstry, Journal of Applied Physics **109**, 064105 (2011).

[45]W. Zhu, I. Fujii, W. Ren, and S. Trolier-McKinstry, Journal of Materials Science **49**, 7883 (2014).

[46]C. Borderon, A. E. Brunier, K. Nadaud, R. Renoud, M. Alexe, and H. W. Gundel, Scientific Reports **7**, 3444 (2017).

[47]M. D. Coulibaly, C. Borderon, R. Renoud, and H. W. Gundel, Journal of Materials Science: Materials in Electronics (2022), 10.1007/s10854-022-09036-5.

[48]K. Nadaud, C. Borderon, R. Renoud, A. Ghalem, A. Crunteanu, L. Huitema, F. Dumas-Bouchiat, P. Marchet, C. Champeaux, and H. W. Gundel, Applied Physics Letters **112**, 262901 (2018).

[49]S. E. Reyes-Lillo and K. M. Rabe, Physical Review B **88**, 180102 (2013).

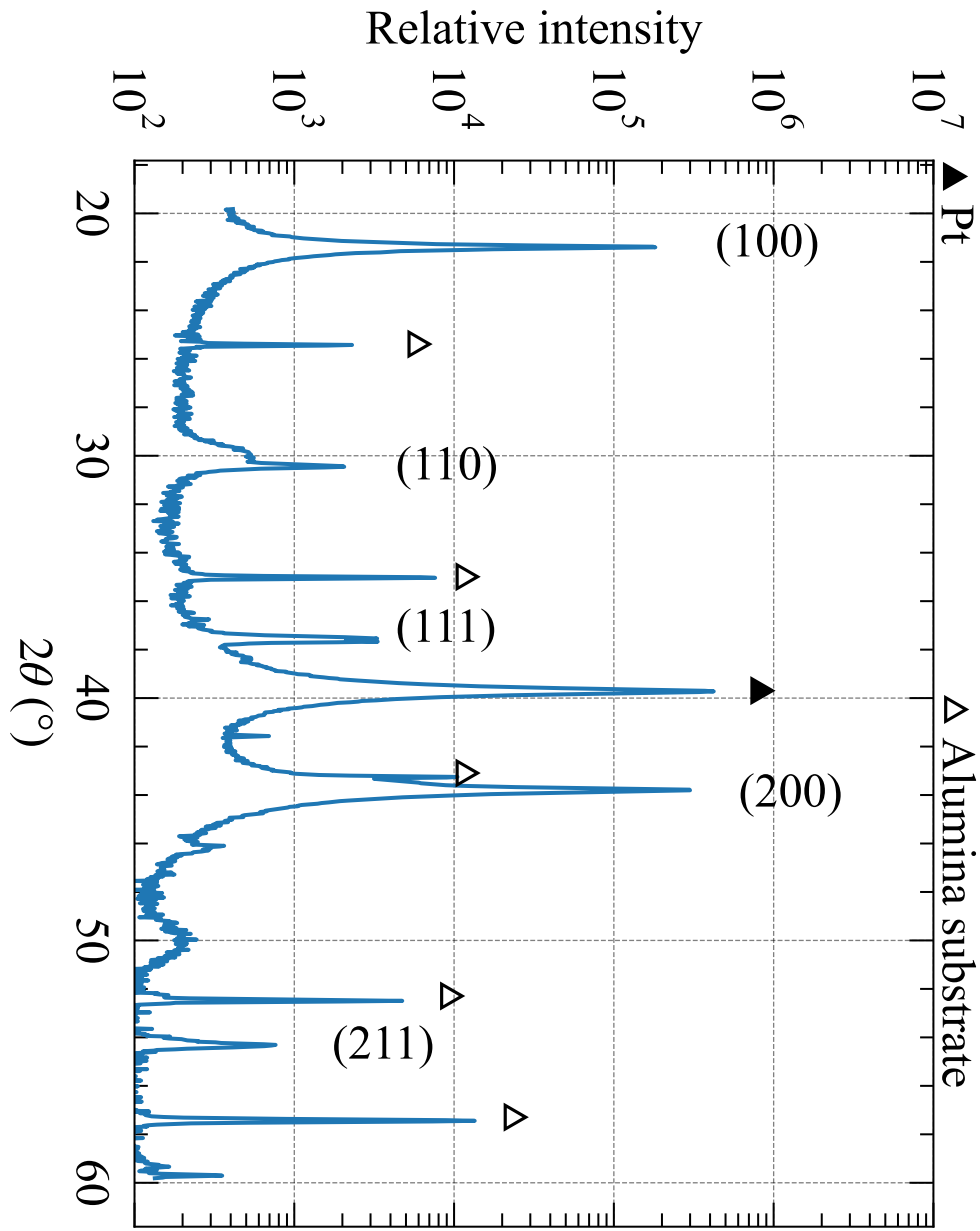

AIP Publishing

Journal of Applied Physics

PLEASE CITE THIS ARTICLE AS DOI: 10.1063/5.0143659

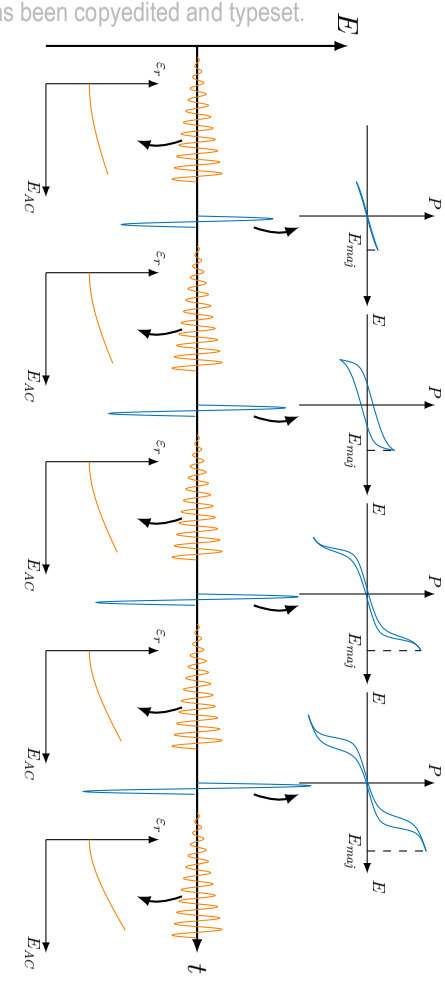

Journal of Applied Physics

AIP Publishing

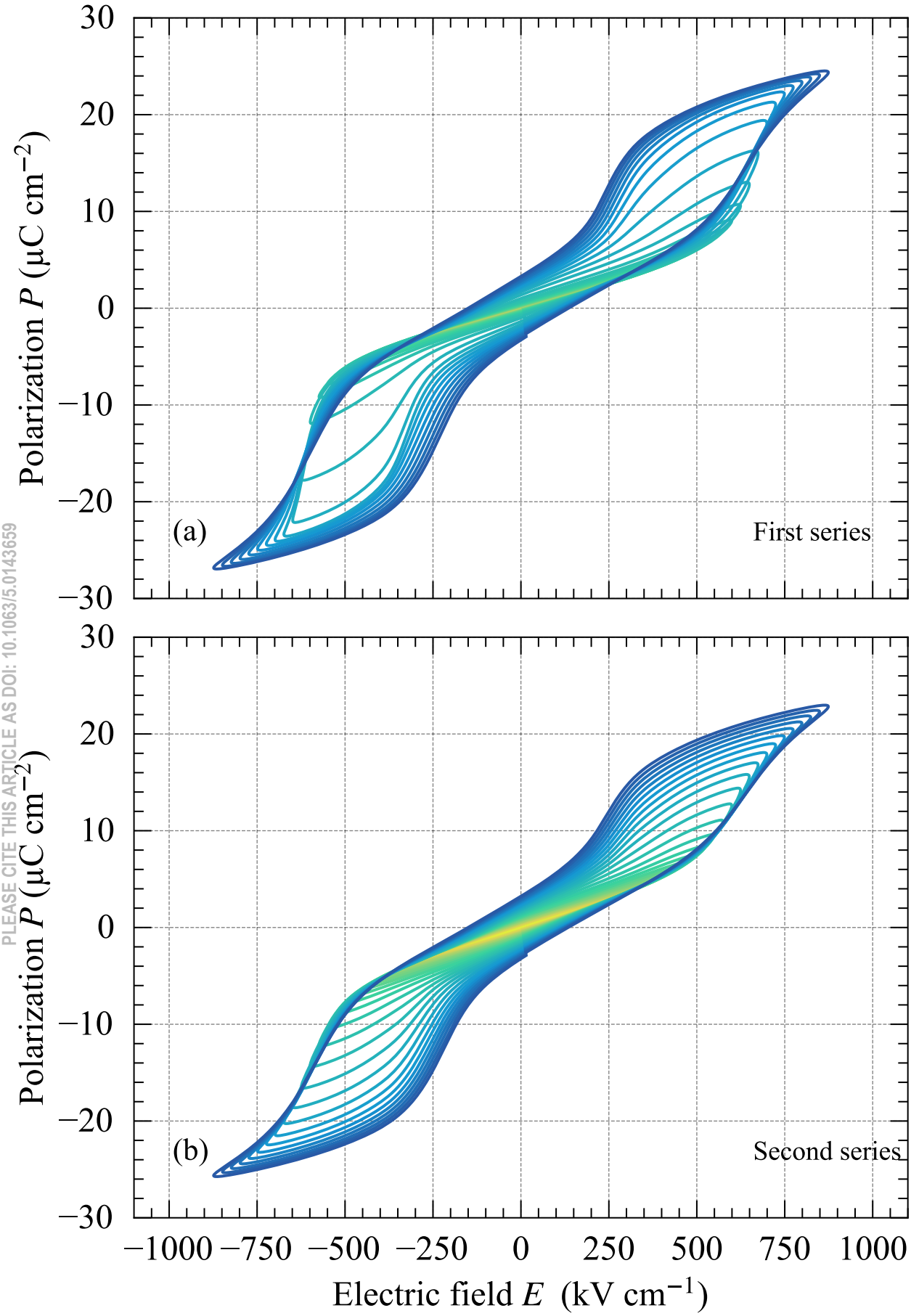

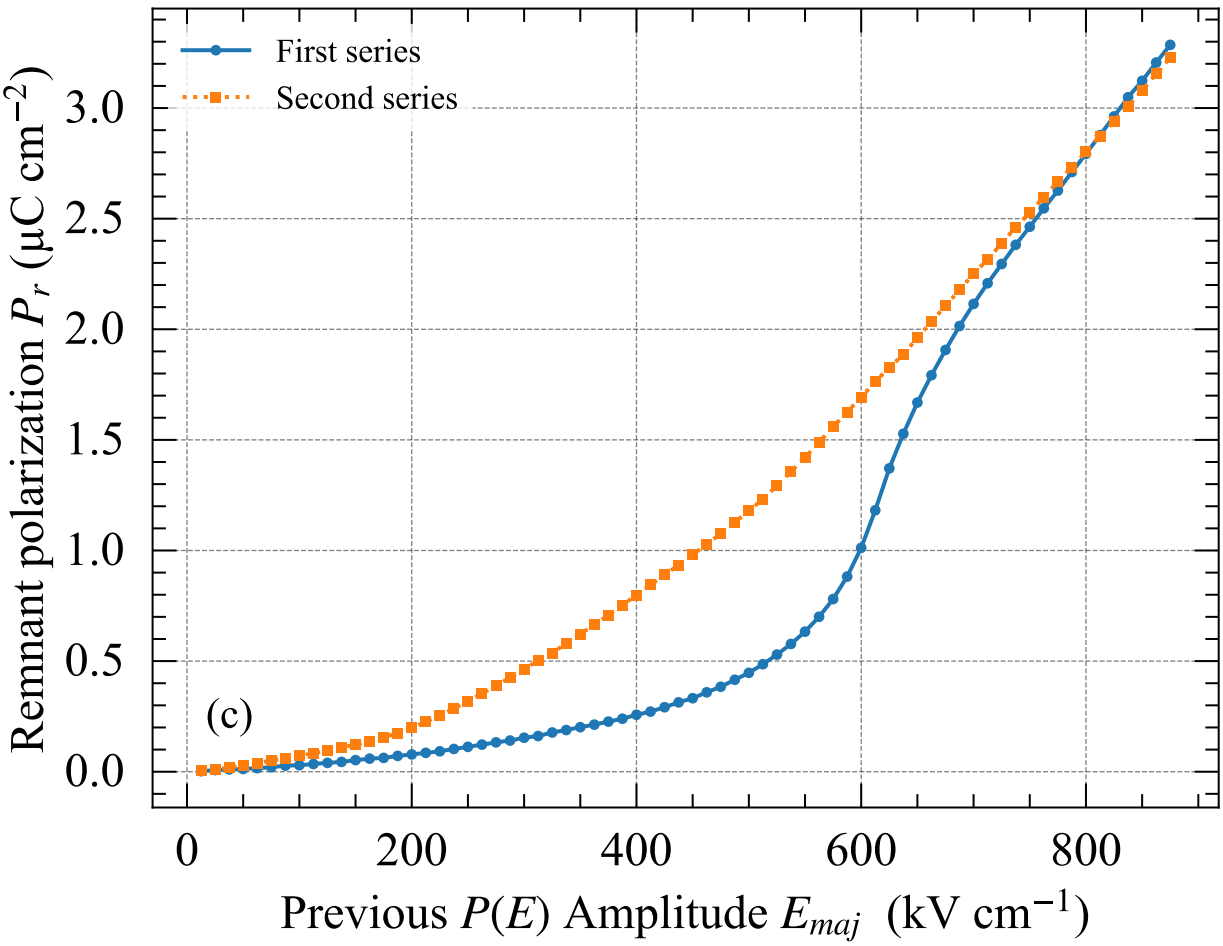

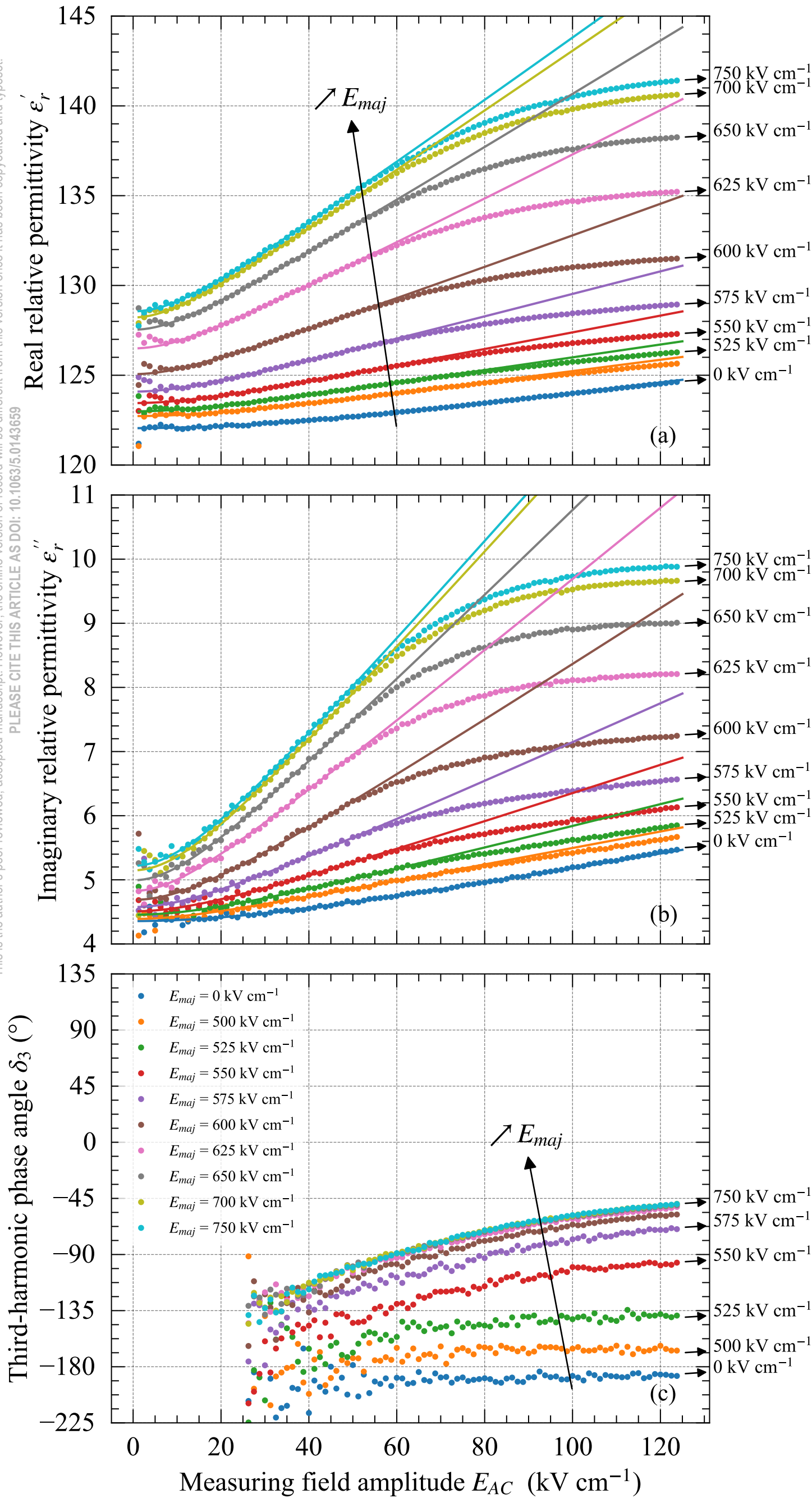

Journal of Applied Physics
AIP Publishing